Thermalization and localization in random unitary circuits

Charles Stahl

April 20, 2019

1 Introduction

In this essay we will discuss the quantum dynamics of closed systems, showing that the two late-time possibilities are thermalization and localization. We will then describe how to study these processes using random unitary circuits. Sec. **??** presents various methods of describing dynamics in thermalizing circuits. The majority of circuits currently described in the literature thermalize, although this is not a necessity. One path to localization in random unitary circuits is through fractonic conservation laws. To motivate these we will introduce fractonic systems in Sec. 6 and show how they naturally conserve higher moments of charges. Finally, in Sec. 7 we will show that circuits that conserve these higher moments of charge indeed localize. We will follow the results of [1], and in fact the first 4 sections of this essay are designed to build to these results. Sec 8 reviews the broad structure of this essay and presents some possibilities for future research.

Include term "scrambling, ergodic"

Always write S_Z as Z?

2 Quantum dynamics of closed systems

This section will serve to introduce the reader to the basics of quantum dynamics of closed systems. It will closely follow Ref. [2], drawing on other sources for examples.

I'll cover operator spreading here, although some of that material may belong in the RUC section. Other sources include [3–5].

2.1 Closed quantum systems

Quantum statistical mechanics usually considers a quantum system coupled to a bath. As in classical statistical mechanics, this allows the system to exchange energy and conserved charges with the bath. Additionally, the system may become entangled with the bath, leading to dephasing. Then, as in the classical case, the state of the system at long time (is—may be approximated by) the thermal state, $\rho^{\text{th}}(T) = Z^{-1}(T)e^{-H/T}$.

Sometimes these systems are integrable...

2.2 Thermalization and localization

Since the bath itself is quantum mechanical, we could consider the system and bath together as a single closed quantum system. We will take this perspective for the remainder of the essay, referring

to the original system as some subsystem. The study of closed quantum systems has expanded recently, driven by experimental, numerical, and theoretical motivations [3].

I'll discuss the ETH here as it seems to be an important enough result, but I don't think it's strictly necessary for the flow of the essay.

I'll continue to follow the Nandkishore review for this section and the section on MBL.

2.3 Operator spreading as a measure of dynamics

How can we measure dynamics? Can we look at how states evolve? This is tempting, but we would need a background...

We will look at how initially local operators spread in time. They will evolve in the Heisenberg picture...

Two measures of the spreading of an operator are the right weight density $\rho_R(i,t)$ and the OTOC $C(i,t)$.

OTO correlator.

2.4 Other measure of dynamics

Other useful quantity is the bipartite entanglement entropy $S(i,t)$. Other possible entropies: Renyi entropies. Dynamics studied in [6, 7]. Also mention [8].

I like the transition between thermalizing and localizing phases, so I'll spend some time on that, with sources [9, 10]. Specifically, the fact that this is not a phase transition of the ground state, like we are used to, and different order parameters for the transition.

3 Random unitary circuits and Floquet systems

In this essay we will be considering the dynamics of Hamiltonian systems, quantum circuits, and Floquet systems. We have already assumed the reader is familiar with the evolution of operators under Hamiltonian dynamics, but here we will introduce quantum circuits and Floquet systems. Both have unitary evolution, but are in some sense less structured than Hamiltonians.

Define "physical" systems, disorder realization.

Haar measure

3.1 Random unitary circuits

Quantum circuits, unsurprisingly, are the quantum analogue of classical circuits. As unitarity is a constraint on quantum evolution, they are also called unitary circuits. We will be interested in

Coarse graining

3.2 Floquet systems

Theres a thorny issue that we brushed asie when we discussed systems without conserved quantities. We defined the systems by their Hamiltonians, but any system with a Hamiltonian conserves energy. As discussed in Sec. 1, random circuits need not have any conserved quantities at all. How then can we compare them to any sort of Hamiltonian system?

The resolution lies in Floquet systems. In this branch of systems, there is a succession of Hamiltonians applied, each for a set amount of time. For example, if we "turn on" Hamiltonian H_1 for time

$T/2$ and then H_2 for $T/2$, then the Floquet unitary time evolution operator for one whole period of time T is

$$U_F(T) = U_2\left(\frac{T}{2}\right)\ U_1\left(\frac{T}{2}\right) = e^{-i\frac{T}{2}H_2}e^{-i\frac{T}{2}H_1}. \tag{1}$$

For $t = nT$ with $n \in \mathbb{Z}$, the time evolution operator is $U(t) = U^n(T)$, while for noninteger multiples of T it is more complicated.

One example is the kicked Ising model [11], with

$$\begin{aligned} H_1 &= \sum_i \left(Z_i Z_{i+1} + g Z_i\right), \\ H_2 &= h \sum_i X_i. \end{aligned} \tag{2}$$

Note that all terms acting at a given time commute with each other. Therefore this Floquet model can be written as a unitary circuit (not random) with 2-site gates.

Another example, from Refs. [12, 13], has time evolution operator

$$U_F(T) = e^{-i\frac{T}{2}H_x}e^{-i\frac{T}{2}H_z}, \tag{3}$$

with

$$\begin{aligned} H_x &= \sum_i g\Gamma X_j, \\ H_z &= \sum_i \left[Z_i Z_{i+1} + (h + g\sqrt{1-\Gamma^2}G_i)Z_i\right], \end{aligned} \tag{4}$$

where G_i are independent Gaussian random variables. We will use the parameters $(g, h, T) = (0.9045, 0.8090, 0.8)$ throughout. Note that as $\Gamma \to 1$ this approaches the kicked Ising model, which thermalizes. As $\Gamma \to 1$, this model becomes equivalent to the time-independent Hamiltonian $H = \sum_i \left[Z_i Z_{i+1} + h_i Z_i\right]$ with random field h_i, which is localized. For lack of a better term we will call Eq. 3 the Γ model.

As in the previous section, we can study the transition between the localized and thermalizing phases by varying a parameter of the model, in this case Γ. Fig. 1 demonstrates the transition using two diagnostics. The first is the entanglement entropy between two halves of the chain in energy eigenstates,

$$S_E \equiv -\operatorname{Tr}\{\rho_L \log \rho_L\} = -\operatorname{Tr}\{\rho_R \log \rho_R\}, \tag{5}$$

where ρ_L and ρ_R are reduced density matrices of the right and left halves of the chain, with no relation to the operator right- and left-weights. The second equality in 5 is due to the whole chain being in a pure state. The maximal possible entanglement between these halves is $S_{\max} = L/2$, but random pure states will be close to the Page value [14, 15]

$$S_R = \frac{L}{2} - \frac{1}{2\ln 2} - \mathcal{O}\left(\frac{1}{2^L}\right). \tag{6}$$

In the thermalizing phase the eigenstates have "volume law" entanglement, close to S_R, while in the localized phase they have "boundary law" entanglement, constant in L [12]. Therefore for large enough L, S_E/S_R should distinguish between the phases. After averaging over all eigenstates

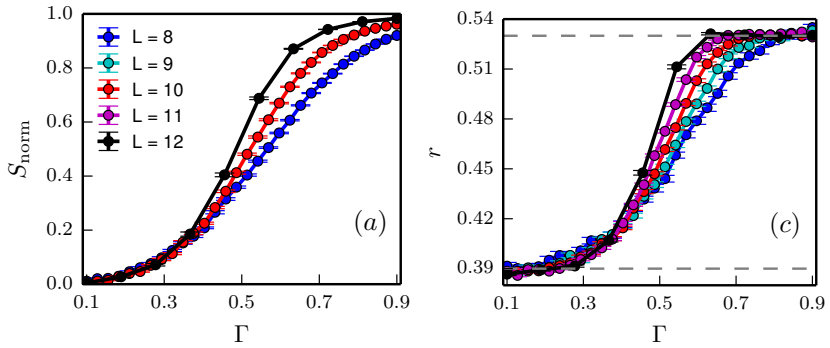

Figure 1: Dynamical phase transition of the Γ model. (a) demonstrates the phase transition through the average entanglement entropy between halves of the chain. (c) shows the same transition, but using the level statistics parameter. Figure from [12].

for a given disorder realization and then averaging over disorder realizations, we arrive at $S_{\rm norm} = \langle S_E \rangle / S_R$.

Alternatively we can use the level statistics parameter r discussed previously. In the thermalizing phase the energies should be distributed according to the circular orthogonal ensemble with $r \approx 0.53$, while in the localizing phase the energies follow Poisson level statistics with $r \approx 0.39$. The dashed lines in Fig. 1 show these values.

In Fig. 1, notice the agreement between the two diagnostics in the critical value Γ_c. Furthermore, both transitions become sharper for increasing L, as one would expect. The suggestion is that the transition is singular in the thermodynamic limit. In Sec. 4.1 we will study this model at $\Gamma = .85$, deep in the thermalizing phase.

4 Thermalization in systems with no conservation laws

This section contains the phenomenology and analysis of thermalization of

4.1 Physical systems with no conservation laws

As shown previously, the Γ model with $\Gamma = 0.85$ is deep within the thermalizing phase. Ref. [13] studied the OTO correlator of an initially local operator in this model. Recall that whereas thermalization is associated with a growing OTOC, it is associated with a decaying OTO correlator.

The key point is the exponential dependence of the OTO correlator. Fig. 2 shows the exponential decay of the OTO correlator for various system sizes. Finite size effects cause the OTO correlator to saturate and therefore deviate from exponential behavior. However, the figure shows that this happens later for larger L, suggesting that the exponential decay continues for an arbitrarily long time for large enough L.

Ref. [11] cranks Γ all the way to 1, to study the kicked Ising model, defined in Eq. 2. It goes beyond the early-time exponential dependence to study the saturation. The quantity under inspection is now the OTOC rather than the OTO correlator, so it should start at 0 and saturate to 1. There is also a focus on the operator right- and left-weights, ρ_L and ρ_R.

Fig. 6 shows the relevant quantities. Although it is for the quantum circuit, the qualitative behavior is the same (that's the whole point of this essay). At each site, exponential growth of both ρ_R and the OTOC begins when the site enters the light cone. Exponential growth continues until the front reaches the site, at which point ρ_R peaks and the OTOC begins to saturate. This front is

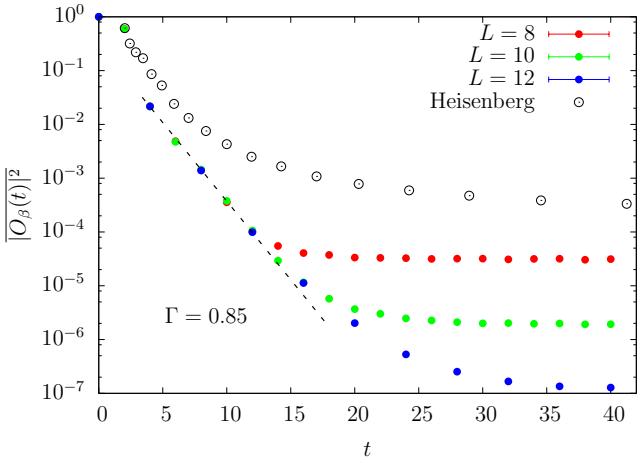

Figure 2: Exponential decay of the OTO correlator in a thermalizing Floquet model with no conserved charges [13]. For increasing system size, the decay continues to be exponential for a longer time before saturating. The black circles show the non-exponential decay of a Hamiltonian system. This decay is power-law, and will be discussed in the following section.

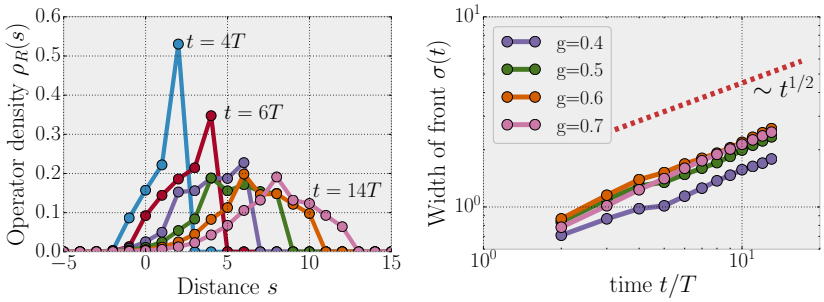

Figure 3: Spreading of peaks in the kicked Ising model [11].

the focus of Ref. [11]. Figs. 6 (a) and (b) can be thought of as horizontal slices though Fig. 6 (c). To compare with Fig. 2, imagine a vertical slice through 6 (c), with $t = 0$ occurring at the position of the light cone.

The results, found through numerical simulation, are that the front propogates linearly at a velocity called the butterfly velocity, v_B. Consider $\rho(i, t)$. For $t << v_B i$, the spreading operator has not yet reached i and $\rho(i, t)$ is small. As the peak passes site i, a significant number of Pauli strings in the operator end on i. In the future, most strings end after i so $\rho_R(i)$ is again small. For a given t, $\rho_R(i)$ peaks at $i = v_B t$. This peak has width $\sim t^\alpha$ [11]. Fig. 3 shows that $\alpha \approx .5$, so that the peaks spread with $\sqrt{t}$. This will be another test of our quantum circuits.

4.2 Circuits with no conservation laws

Early exponential growth. Presence of front. Broadening of front and exponential dependence therein.

The circuit under investigation in this section has the same architecture as Fig. **??**, with each gate chosen from the Haar measure. Our goal is to find the dynamics of ρ_R under the action of the full circuit, and our analysis will follow [11]. The first step in doing so is to calculate the dynamics of ρ_R under a single gate.

We want to calculate $\rho_R(i, \tau + 1)$ and $\rho_R(i + 1, \tau + 1)$ (Fig. 4). It should be clear that these

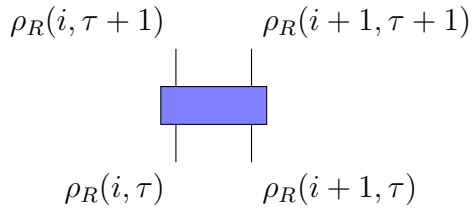

Figure 4: Diagram of the operator weights before and after the application of the gate. Values at $\tau+1$ are calculated in the text.

quantities only depend on $\rho_R(i,\tau)$ and $\rho_R(i+1,\tau)$. In fact it is even simpler, in that $\rho_R(i,\tau+1)$ and $\rho_R(i+1,\tau+1)$ only depend on the sum $\rho_R(i,\tau)+\rho_R(i+1,\tau)$.

Looking at $\rho_R(i,\tau)$ and $\rho_R(i+1,\tau)$ is equivalent to looking only at Pauli strings which are I on all sites past $i+1$ but are non-identity on either i or $i+1$ (or both). This leaves us with q^4-1 two-site operators to consider. The Haar-random gate transforms any of these operators to any other with equal probability [16], regardless of whether the initial operator was an identity on site $i+1$. This is why the final values only depend on $\rho_R(i,\tau)+\rho_R(i+1,\tau)$.

Of the q^4+1 final operators, q^2-1 are the identity on site $i+1$. These operators contribute to $\rho_R(i,\tau+1)$, while the rest contribute to $\rho_R(i+1,\tau+1)$. In other words the weight moves to site i with probability $p_{\text{back}}=\frac{q^2-1}{q^4-1}=\frac{1}{q^2+1}$ or moves forward with probability $p\equiv 1-p_{\text{back}}=\frac{q^2}{q^2+1}$. Thus

$$\begin{aligned}\rho(i,\tau+1)&=(1-p)\left[\rho(i,\tau)+\rho(i+1,\tau)\right],\\ \rho(i+1,\tau+1)&=p\left[\rho(i,\tau)+\rho(i+1,\tau)\right].\end{aligned}\tag{7}$$

This is true at each individual gate. If there were a gate at each site at each time, this would be the final word. However, since the dynamics will only be periodic in every two layers of the circuit, we must calculate the dynamics for two layers to get the whole picture.

To do so, we will define some dense but useful notation. Since the sum of weights at consecutive sites is so important, we will abbreviate it as

$$\tilde{\rho}_R(i,\tau)\equiv\rho_R(i,\tau)+\rho_R(i+1,\tau).\tag{8}$$

We will want to find $\tilde{\rho}_R(i,\tau+2)$. To do so we find

$$\begin{aligned}\rho_R(i-1,\tau+1)&=p\tilde{\rho}_R(i-2,\tau),\\ \rho_R(i,\tau+1)&=(1-p)\tilde{\rho}_R(i,\tau),\\ \rho_R(i+1,\tau+1)&=p\tilde{\rho}_R(i,\tau),\\ \rho_R(i+2,\tau+1)&=(1-p)\tilde{\rho}_R(i+2,\tau).\end{aligned}\tag{9}$$

Similar calculation at time $\tau+2$ result in

$$\begin{aligned}\rho_R(i,\tau+2)&=p^2\tilde{\rho}_R(1-2,\tau)+p(1-p)\tilde{\rho}_R(i,\tau),\\ \rho_R(i+1,\tau+2)&=p(1-p)\tilde{\rho}_R(i,\tau)+(1-p)^2\tilde{\rho}_R(i+2,\tau),\\ \tilde{\rho}_R(i,\tau+1)&=p^2\tilde{\rho}_R(i-2,\tau)+2p(1-p)\tilde{\rho}_R(i,\tau)+(1-p)^2\tilde{\rho}_R(i+2,\tau).\end{aligned}\tag{10}$$

Fig. 5 shows a diagram containing these values.

The fact that $i\pm1$ and $\tau\pm1$ do not appear in Eq. 10 demonstrates the usefulness of the coarse-grained variables, defined in Fig. **??**. Switching to those variable and dropping the tilde, Eq 10 becomes

$$\rho_R(x,t+1)=p^2\rho_R(x-1,t)+2p(1-p)\rho_R(x,t)+(1-p)^2\rho_R(x+1,t),\tag{11}$$

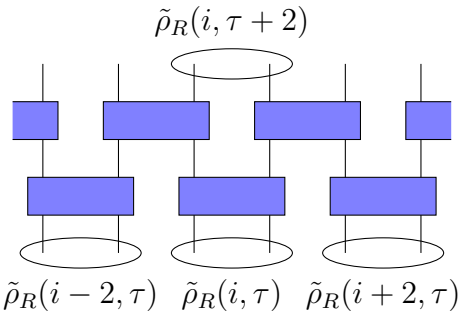

Figure 5: Operator weights after two layers of the circuit

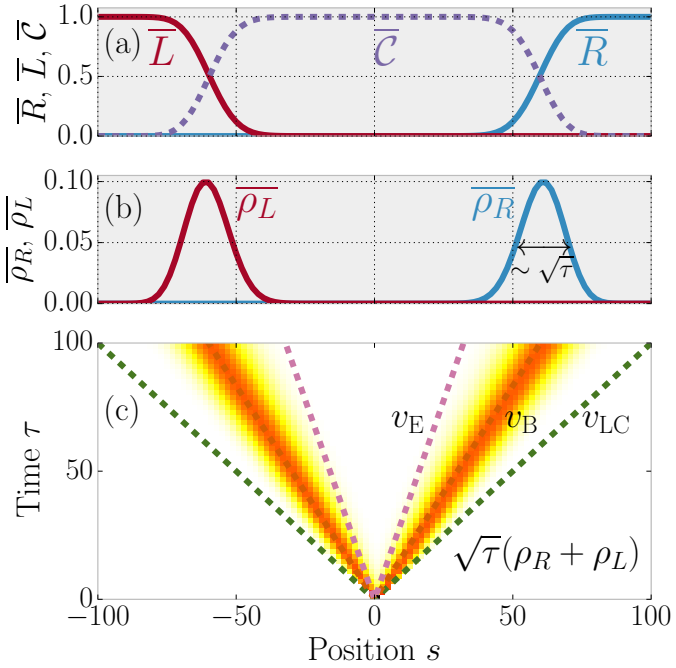

Figure 6: Spreading of an initially local operator under a quantum circuit with no conservation laws [11].

which is the equation for a biased random walk that steps to the right with probability p^2 and to the left with probability $(1-p)^2$, otherwise staying at the same site.

Therefore, for any operator initially local at position x_0, ρ_R spreads linearly with a front located near position $x = x_0 + v_B t$. The front spreads diffusively as $\langle x^2 \rangle - \langle x \rangle^2 = 2Dt$ [11]. The values are

$$\begin{aligned} v_B &= p^2 - (1-p)^2 = \frac{q^2-1}{q^2+1}, \\ D &= \sqrt{1-v_B^2}/4 = \frac{q/2}{q^2+1}. \end{aligned} \tag{12}$$

These results can be summarized in Fig. 6. As an interesting aside, note that in the large q limit the front does not diffuse and $v_B = 1$, the lightcone velocity [17].

The important features that we can match to the behavior of the floquet model are the exponential growth at early time and the behavior of the front of the spreading operator. As in the kicked Ising model, we have shown that the front moves linearly. The diffusion process has a width $\sim \sqrt{Dt}$, which is to say $\alpha = 0.5$

vonKeyserlingk page 6.

5 Thermalization in systems with conservation laws

Introducing conserved charges to our systems slows down their dynamics. In this section we will see how this process occurs, in both physical systems and quantum circuits. It is straightforward to introduce conserved charges to the circuits by restricting to gates that satisfy some conservation law. For the physical systems we have two ways to proceed. We can either consider Floquet systems with conservation laws, or systems with time-independent Hamiltonians (with or without further conservation laws).

5.1 Floquet systems with conserved quntities

We can introduce conserved charges to Floquet systems by ensuring that both partial Hamiltonians in the model obey some conservation law. Ref. [18] studies a model with time evolution operator

$$U_F(T) = e^{i\frac{T}{2}H_z} e^{i\frac{T}{2}H_{xy}}, \tag{13}$$

where

$$\begin{aligned} H_z &= J_z \sum_i Z_i Z_{i+1}, \\ H_{xy} &= J_{xy} \sum_i \left[X_i X_{i+1} + Y_i Y_{i+1} \right]. \end{aligned} \tag{14}$$

In these "physical systems," it is possible to have approximately conserved charges, i.e. on the localized side of a phase transition...

5.2 Constrained circuits and conserved operators

A simple conservation law to introduce to quantum circuits is conservation of total Z. We simply have to constrain the 2-site gates to conserve Z_{tot} for the two sites on which it acts. Z_{tot} is then our conserved charge, with charge density Z_i. We will use spin-$\frac{1}{2}$ sites, so gates will be in the $\uparrow\uparrow\to\uparrow\uparrow$, $\downarrow\downarrow\to\downarrow\downarrow$, or $\{\uparrow\downarrow,\downarrow\uparrow\} \to \{\uparrow\downarrow,\downarrow\uparrow\}$ sectors. We will refer to these as the $Z = 1$, $Z = 0$, and $Z = -1$ sectors, of dimension 1, 4, and 1, respectively. The matrix representations of gates will be 4×4 matrices made up of three block matrices, one for each sector.

Like in the unconstrained circuit, we want to have an on-site dimension q that we can use to vary the behavior of the circuit. It would also be nice to preserve the block structure of the gates as we vary q, which would not be possible if we replace the spin-$\frac{1}{2}$ sites with higher spin. We can satisfy both of these requests by instead replacing the spins with a tensor product between a spin-$\frac{1}{2}$ degree of freedom and an unconstrained q-dimensional qudit. We do not constrain the gates' action on the qudits. This leaves us with $4q^2 \times 4q^2$ block-diagonal gates, with blocks of size $q^2 \times q^2$, $2q^2 \times 2q^2$, and $q^2 \times q^2$ (Fig. 7).

The next step is to define a basis for our operators. On the qudit, we will continue to use an abstract Pauli basis Σ_i^ν, $\nu = 0, \ldots, q^2 - 1$. On the qubit, instead of the usual Pauli operators, we will use the basis [18]

$$\{\sigma_i^{\mu=0,1,2,3}\} \equiv \{I_i, R_i, L_i, Z_i\} = \{I_i, \frac{\sigma_i^+}{\sqrt{2}}, \frac{\sigma_i^-}{\sqrt{2}}, \sigma_i^z\} \tag{15}$$

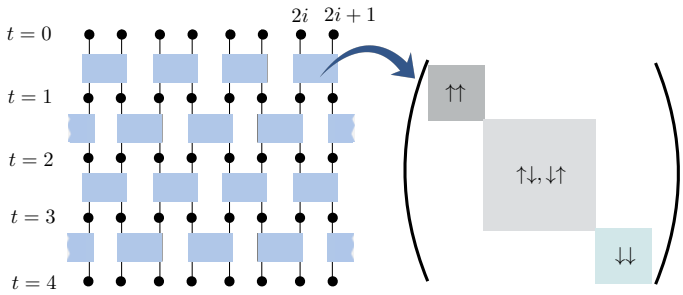

Figure 7: A quantum circuit constrained to conserve Z_{tot}. The three blocks are of dimension $q^2 \times q^2$, $2q^2 \times 2q^2$, and $q^2 \times q^2$. Figure from [18].

We have chosen σ_i^1, σ_i^2 to be normalized raising/lowering operators, or equivalently charge creation/annihilation operators. Then the basis on site i is $B_i^{\mu\nu} \equiv \sigma_i^\mu \otimes \Sigma_i^\nu$. We will write these as $(I\Sigma^\nu)_i$, $(Z\Sigma^\nu)_i$, etc. The basis strings will be of the form $\mathcal{S} = \otimes_i B_i^{\mu_i\nu_i}$.

Some operators are special because they measure the conserved charge. The local charge density is $Z_i = (ZI)_i$, while the total charge is $Z_{\text{tot}} = \sum_i (ZI)_i$. Charge conservation is written as

$$Z_{\text{tot}}(t) = U(t)^\dagger Z_{\text{tot}}(0) U(t) = Z_{\text{tot}}(0), \tag{16}$$

where $U(t)$ is the combined action of the entire circuit.

Along the way to defining the right-weight, we defined the operator amplitude

$$a_{\mathcal{S}}(t) = \frac{1}{q^L} \text{Tr}\{\mathcal{O}(t)\mathcal{S}\}, \quad \sum_S |a_{\mathcal{S}}| = 1, \tag{17}$$

with the latter equality imposed by unitarity. For the new conserved charge we can define the conserved operator amplitude,

$$a_i^c(t) = \frac{1}{(2q)^L} \text{Tr}\{\mathcal{O}(t)(ZI)_i\}, \tag{18}$$

and the "conserved part" of $\mathcal{O}(t)$,

$$\mathcal{O}^c(t) = \sum_i a_i(t)(ZI)_i. \tag{19}$$

The conservation law (16) is then equivalent to

$$\sum_i a_i^c(t) = \sum_i a_i^c(0). \tag{20}$$

Note that Eq. 20 refers to amplitudes, while Eq. 17 refers to squares of amplitudes. Later, we will also want to refer to the conserved and nonconserved right-weights,

$$\rho^c(i,t) = \left|a_i^c(t)^2\right|, \quad \rho_R^{\text{nc}}(i,t) = \rho_R(i,t) - \rho^c(i,t). \tag{21}$$

5.3 Operator spreading in conserving circuits

We are now ready to discuss the spreading of operators. We will consider the operator $(ZI)_0$ where $i = 0$ is the middle of a long chain. There will be three behaviors extracted from our model: diffusion

of the conserved operators (forming a "lump"), ballistic propagation of the "front" of nonconserved operators, and a power-law "tail" of nonconserved operators behind the front. Fig. 8 illustrates these three regimes.

We'll start with the conserved operators. The effect of a Haar-random unitary acting on sites i and $i+1$ is to average the conserved amplitudes, so that

$$a_i^c(t+1) = a_{i+1}^c(t+1) = \frac{a_i^c(t) + a_{i+1}^c(t)}{2}, \tag{22}$$

where equality holds after Haar-averaging.[1] After coarse graining $i \to x$, in the $x, \to \infty$ limit, this behavior results in

$$a^c(x,t) = \sqrt{\frac{1}{2\pi t}} e^{-\frac{x^2}{2t}}, \tag{23}$$

which is a diffusing lump with diffusion constant $D_c = \frac{1}{2}$. Therefore the total weight on conserved operators falls over time,

$$\rho_{\text{tot}}^c(t) \simeq \int dx\ |a^c(x,t)| = \int dx\ \frac{1}{2\pi t} e^{-x^2/t} = \frac{1}{2\sqrt{\pi t}}, \tag{24}$$

with power-law dependence.

If ρ^c is decreasing, then ρ^{nc} must be increasing. The effect of Eq. 22 is to decrease $\rho^c(i,t)$ by

$$\delta\rho_i^c(t) = -\frac{(a_i^c(t) - a_{i+1}^c(t))^2}{2}. \tag{25}$$

All of this weight gets shuffled into nonconserved operators. But we know how nonconserved operators spread! In fact, we can simply use the analysis of the previous section to say that there is a front that travels at v_B, broadening diffusively with width $\sim \sqrt{D_\rho t} \sim \sqrt{t/q^2}$. In the large q limit, the diffusivity vanishes and therefore the front has zero width.

If there were no remaining lump at the origin, our description of the front would be complete. However, even at late time the lump of conserved operators is emitting nonconerved operators. These operators form a tail lagging behind the front. Since the lump shrinks as a power law in time and all nonconserved operators travel at $\sim v_B$, the tail has a power-law shape in space. In fact, at time t and position x, with x well separated from the origin and from $v_B t$, the majority of $\rho_R^{\text{nc}}(x,t)$ comes from operators emitted from the lump at time $t - x/v_B$. If the lump is far away, it can be approximated by a point source with all weight at the origin, emitting nonconserved operators proportional to the decrease in ρ_{tot}^c. So,

$$\rho_R^{\text{nc}}(x,t) \sim \frac{\partial \rho_{\text{tot}}^c(t - x/v_B)}{\partial t} \sim \frac{1}{(t - x/v_B)^{3/2}}. \tag{26}$$

The fact that the spacial exponent $-3/2$ is equal to $-1/2 - 1$, where $-1/2$ is the time exponent of the decrease of ρ_{tot}^c, will become important in our analysis of the fracton circuit.

Since this analysis became abstract rather quickly, Fig. 8 shows the qualitative pictures for operators spreading. It includes the large q (ideal) behavior for conserving and nonconserving circuits and also shows how finite q affects these values. The first subfigure shows the lump, front, and tail, while some or all of those features are absent in other systems.

[1] We will we be cavalier about our Haar-averaging. For exact statements see Ref. [18].

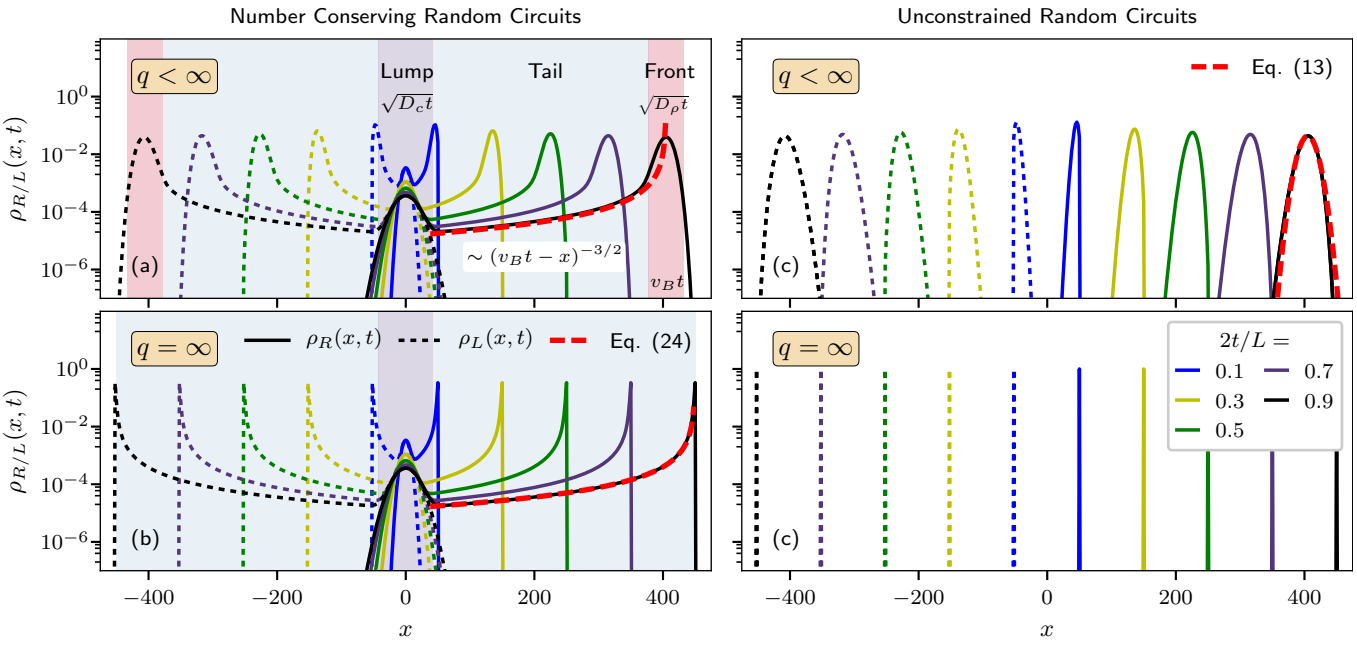

Figure 8: Comparison of circuits with and without conservation laws, at finite and infinite q. Each solid line is a right-weight and each dashed line (except red) is a left-weight. (a): the vertical shading corresponds to the three parts of the operator at $2t/L = 0.9$, the lump, the tail, and the front. The lump consists of conserved operators and broadens diffusively. The front consists of nonconserved operators emitted at early time and travels ballistically. The tail consists of nonconserved operators emitted at later time and has approximate power-law behavior $\sim (v_B t - |x|)^{-3/2}$ (shown by the red dashed line). (b): In the large q limit, the front has width $= 0$ and does not broaden at all (just as in the nonconserving circuit). (c,d): In the nonconserving circuit there are no conserved operators and therefore no central lump. Since the power-law tail is emitted by the lump, there is no such tail in this case either. The only structure is broadening front. As discussed previously, the front does not broaden in the large q limit. Figure from [18].

Now that we have fully described the operator spreading for conserving circuits, we are ready to explain the power-law dependence of the OTO correlator in Sec 5.1. We will use the language of the OTOC, though, because this is the quantity more commonly seen in the literature now.

Once the operator front is far past x ($v_B t >> |x| + \sqrt{D_\rho t}$), most strings that have spread past x look random, so they contribute to the equilibrium value of the OTOC,[2] which is 1. The deviation from the equilibrium value can only be due to operators that have not yet reached x at time t, so they must have been at the origin at time $t' = t - x/v_B$. Since the only operators at the origin are the conserved operators, so using (22) we have

$$1 - C(x,t) = \rho^c_{\text{tot}}(t - x/v_B) = \frac{1}{2\sqrt{\pi(t - x/v_B)}}. \tag{27}$$

Since the OTOC and the OTO correlator are linearly related (**??**), this explains the power-law dependence in Sec 5.1.

The material so far has introduced all of the dynamics-based material we will need to understand fractonic circuits, but we haven't covered fractons yet! We'll take a brief tour into the physics of fractons before circling back to see how we can understand localization in fractonic circuits using our previous analysis of thermalizing circuits.

6 Fractonic systems

In this section we will explore various fractonic systems. We will start with exactly solvable models and show that these naturally result in massive (gapped) fractons. However we will quickly transition to tensor gauge theory, where we can create gapless fractons. Ultimately, we want to show the connection between multipole conservation laws (specifically dipole) and fractons. This motivates the study of random circuits that conserve dipole moment as a setting for localized charges, which will be presented in Sec. 7.

The conservation of dipole moment means that an isolated charge cannot move without creating an isolated dipole somewhere else, which costs energy. Thus, the charges are immobile in the low-energy limit.

6.1 Tensor gauge theory

We will show how fracton conservation laws naturally lead to tensor gauge theory. Although this is not strictly necessary to understand the dynamics of fracton systems, the literature often refers to fractons using the language of tensor gauge theory. This discussion follows the treatment in [19].

To start, we will briefly review the familiar form of U(1) gauge theory. Consider a complex scalar field $\phi(x,t)$. We will treat time and space separately despite the theory being Lorentz invariant because the fracton theory is not Lorentz invariant. The charge density of this field is $\rho = \phi^\dagger\phi$, with total charge $Q = \int d^dx\rho$. Requiring $Q = \text{const.}$ is equivalent to requiring

$$\phi \to e^{i\alpha}\phi \tag{28}$$

be a symmetry of the theory, for constant α. At this point ϕ and all of its derivatives and powers transform covariantly, which is to say that each operator transforms as $\mathcal{O} \to e^{in\alpha}\mathcal{O}$ under the phase rotation.

[2] This is a simplification. See [18] for details

Gauging this theory requires that the theory be invariant under $\phi \to e^{i\alpha(x,t)}\phi$ for arbitrary $\alpha(x,t)$. However, the derivative of the field now transforms as

$$\begin{aligned}\partial_i\phi &\to e^{i\alpha}\left(\partial_i + \partial_i\alpha\right)\phi,\\ \partial_t\phi &\to e^{i\alpha}\left(\partial_t + \partial_t\alpha\right)\phi.\end{aligned} \tag{29}$$

This is not a covariant transformation, as it mixes the derivatives of ϕ with ϕ itself. The standard solution is to introduce gauge derivatives $D_i = \partial_i - iA_i$ and $D_t = \partial_t - i\Phi$, where Φ recalls the notation for the scalar potential of electromagnetism. We then have

$$\begin{aligned}D_i\phi &\to e^{i\alpha}D_i\phi,\\ D_t\phi &\to e^{i\alpha}D_t\phi,\end{aligned} \tag{30}$$

if

$$\begin{aligned}A_i &\to A_i + \partial_i\alpha,\\ \Phi &\to \Phi + \partial_t\alpha.\end{aligned} \tag{31}$$

We can then go on to calculate field strengths and possible terms in the action, but our main interest is in the fact that the gauge field is a spacetime vector $A_\mu = (\Phi, A_i)$. For more details see [19].

We will now go through the same steps for a fracton field ϕ in order to show the natural emergence of symmetric tensor gauge fields. ϕ is again a complex scalar that conserves charge $Q = \int d^dx\rho$. It also conserves dipole moment $P_i = \int d^dx\rho x^i$ (breaking Lorentz invariance). Together these correspond to phase rotations of the form

$$\phi \to e^{i\alpha + i\lambda_i x^i}\phi. \tag{32}$$

We will write this phase as $e^{i\alpha(x)}$ where α is restricted to be linear until we gauge the theory.

Now $\partial_i\phi \to e^{i\alpha}(\partial_i + \lambda_i)\phi$ is no longer covariant. The second derivative

$$\partial_i\partial_j\phi \to e^{i\alpha}(\partial_i\partial_j + \lambda_i\partial_j + \lambda_j\partial_i)\phi \tag{33}$$

looks slightly more promising because its symmetric structure can also be obtained from the operator $\partial_i\phi\partial_j\phi$. In fact, the lowest order operator is [19]

$$\phi\partial_i\partial_j\phi - \partial_i\phi\partial_j\phi \to e^{2i\alpha}\left(\phi\partial_i\partial_j\phi - \partial_i\phi\partial_j\phi\right). \tag{34}$$

This means that the action can contain this operator.

Gauging the fracton theory so that α is again an arbitrary function, we now find

$$\phi\partial_i\partial_j\phi - \partial_i\phi\partial_j\phi \to e^{2i\alpha}\left(\phi\partial_i\partial_j\phi - \partial_i\phi\partial_j\phi + i(\partial_i\partial_j\alpha)\phi^2\right). \tag{35}$$

This suggests that, instead of constructing the covariant first derivative $D_i\phi$, we construct a covariant second derivative

$$D_{ij}\phi^2 = \phi\partial_i\partial_j\phi - \partial_i\phi\partial_j\phi + iA_{ij}\phi^2, \tag{36}$$

where this is shorthand for D_{ij} being a bilinear derivative operator acting on two copies of the field ϕ. This operator transforms covariantly if

$$A_{ij} \to A_{ij} + \partial_i\partial_j\alpha. \tag{37}$$

This transformation law requires A_{ij} to be symmetric, and we have found our symmetric tensor gauge field.

The theory still contains a scalar gauge field $\Phi \to \Phi + \partial_t\alpha$. For the construction of the lowest order Lagrangian of this theory, and other possible symmetric tensor gauge theories, see [19].

6.2 More on fractons

(I'll then discuss this model more, including the difference between the discrete and continuous cases. I'll also present some of the connections to elasticity and gravity, such as in [20].)

7 Localization in fractonic circuits

This section will mostly cover the results in [1]. I'll go through their analytic results and show that their numerics match up. I'd prefer not to do my own numerics because I assume anything I can do in the next month and a half will be a subset of what they achieved, but if you think my essay would benefit from some validation of their numerics at lower L, then I'll go for it.

Since the dipole density is a conserved charge whose higher moments are not conserved, it should behave the way that charge density did in the ergodic charge conserving circuit.

The entirety of this section is based on the work in [1].

7.1 Random walks in $d = 1$

The diffusion operator is $\mathcal{D} = \partial_t - D\partial_x^2$, where D is the diffusion constant. Consider the function $G(x,t) = (4\pi Dt)^{-d/2} e^{-x^2/4Dt}$. We can see that $\mathcal{D}G(x,t) = 0$ for $t > 0$

$$\partial_t G(x,t) = \quad (4\pi D)^{-\frac{d}{2}} \left[-\frac{d}{2} t^{-\frac{d}{2}-1} + t^{-\frac{d}{2}} \frac{x^2}{4Dt^2} \right] e^{\frac{-x^2}{4Dt}}, \tag{38}$$

$$\begin{aligned} D\partial_x^2 G(x,t) &= D(4\pi D)^{-\frac{d}{2}} \vec{\partial}_x \cdot \frac{-\vec{x}}{2Dt} e^{\frac{-x^2}{4Dt}} \\ &= D(4\pi D)^{-\frac{d}{2}} \left[-\frac{d}{2D} t^{-\frac{d}{2}-1} + t^{-\frac{d}{2}} \frac{x^2}{4D^2t^2} \right] e^{\frac{-x^2}{4Dt}}, \end{aligned} \tag{39}$$

$$\mathcal{D}G(x,t) = 0. \tag{40}$$

Furthermore, at early time we have $G(x,t) \xrightarrow[t\to 0]{} \delta(x)$:

$$G(x,0) = 0, \quad x \neq 0, \tag{41}$$

$$\int dx\, G(x,t) = (4\pi Dt)^{-d/2} (4\pi Dt)^{d/2} = 1 \quad \forall t, \tag{42}$$

so $G(x,t)$ acts as a Green's function, or propagator, for the diffusion kernel.

From this function we can estimate how long it takes for a randomly walking particle to return to the origin, the return time t_{return}. This is done by setting an arbitrarily high constant C, and finding at what time the integrated propagator at the origin reaches that value. For $d = 1$,

$$C = \int_0^{t_{\text{return}}} dt\, G(0,t) \tag{43}$$

$$= \int_0^{t_{\text{return}}} dt\, (4\pi Dt)^{-1/2} \tag{44}$$

$$= \sqrt{\frac{t_{\text{return}}}{\pi D}}, \tag{45}$$

or $t_{\text{return}} = \pi D C^2$. In $d = 2$, $t_{\text{return}} = \exp(4\pi DC)$, while for larger d, $t_{\text{return}} = \infty$, which is to say the particle never returns to the origin.

At equilibrium, the particle density will be spread out over a region with length scale $\xi \sim \sqrt{Dt_{\text{return}}}$ (Why?). We will use these facts in the analysis of continuous fracton systems in the next subsection.

7.2 Analytic predictions

Here we will make analytic predictions for the dynamics of a fracton system in continuous time and space before showing that they match numeric simulations for a fractonic quantum circuit with discrete time and space. We will do this only for $d = 1$ systems, but Ref. [1] includes calculations for general d.

Start by recalling that fractons (charges) are indeed mobile, but dipole conservation requires that the movement of a fracton is paired with the creation of a dipole. These dipoles are then free to move, and in fact they diffuse randomly (hence our previous discussion of diffusion). Say the fracton, with unit negative charge, starts at the origin, and call its position R. Since we are in $d = 1$, quantities like position and dipole strength will be scalars.

Consider the creation of a single dipole of magnitude R. In $d = 1$, a random walk returns to the origin in time $\sim D$. When the dipole returns to the location of the fracton, the fracton reabsorbs the dipole, returning to the origin. Thus in $d = 1$ the fracton stays near the origin, constantly emitting and reabsorbing dipoles. We can think of this situation as a diffusing dipole field, with the fracton acting as a source and sink. This results in the equation

$$\frac{\partial \eta}{\partial t}(x) = D\frac{\partial^2 \eta(x)}{\partial x^2} + \frac{dR}{dt}\delta(x - R), \tag{46}$$

where η is the local dipole density.

If initially the fracton is at the origin and no dipoles are present, then the total dipole required to balance out the charge is $\tilde{\eta} = R$. The dipole density at the location of the fracton is $\eta = \tilde{\eta}/\xi$. Thus the fracton equation of motion is

$$\frac{dR}{dt} = -\eta(R) + A(t) \tag{47}$$

$$= \frac{-R}{\sqrt{\pi}DC} + A(t), \tag{48}$$

where $A(t)$ is a random force satisfying $\langle A(t)A(t')\rangle = 2T\delta(t - t')$. The units are very wonky here. This is a Langavin equation [21]. The probability distribution for the fracton to be distance R from the origin has solution

$$P(R) \sim \exp\left(\frac{R^2}{2\sqrt{\pi}DCT}\right), \tag{49}$$

where T is the strength of the random force.

There are few prediction that we can test against in the numerical simulation of the circuit. The zeroth prediction is that the fractons are localized. The first is that the tails of fracton density away from the origin (but within the operator spreading front) should take the form of Eq. 49. Second, as in Eq. 49, the correlation length of fracton density should scale as $\xi_{\text{fracton}} \sim \sqrt{DT}$ as the diffusion constant and force strength change.

The other predictions relate to the shape of evolving dipole and fracton operators. Since the dipole density behaves like a simple conserved charge, its operator spreading should look like that in Sec. 5. In particular, for an initially local dipole operator, there should be a linearly propagating front that broadens as $\sqrt{t}$, with a power-law tail behind the front. As in Sec 5, the exponent for this tail is $-3/2$.

The spreading of an initially local fracton operator shares the universal structure. There is a lump at the origin corresponding to fracton operators (does this decrease in time?), along with another lump at the origin corresponding to dipole operators. The dipole operators are emitted by the fracton

operators in the same way that nonconserved operators are emitted by conserved operators in Sec 5. However, since the dipole operators are also conserved, they do not propagate ($v_{B,\text{dip}} = 0$) and this dipole lump remains at the origin.

The dipole operators at the origin have amplitude [1]

$$a^c(x,t) \sim \frac{x}{t^{3/2}} e^{-x^2/Dt} \tag{50}$$

so the total weight in the dipole lump is

$$\rho^c_{\text{tot}}(t) \sim \int dx \ |a^c(x,t| \sim t^{-3/2}. \tag{51}$$

The analogue of (26) is then

$$\rho^{\text{nc}}_R(x,t) \sim \frac{\partial \rho^c_{\text{tot}}(t - x/v_B)}{\partial t} \sim \frac{1}{(t - x/v_B)^{5/2}}, \tag{52}$$

which is the same as in the thermalizing circuit, except with an exponent of $-5/2$. We will say that the third prediction is (51) and the fourth prediction is the power-law tail with exponent $-3/2$ for dipole operators and $-5/2$ for fracton operators.

The analysis of this section suggests that fractons in a circuit should be localized. It might seem sufficient to simply simulate the circuit and see if the fractons are indeed localized. However, these simulations are limited in system size and simulation time. The extra predictions allow detailed testing of the analytic theory. If all predictions check out, the mechanism behind localization is probably correct, providing a stronger check on the robustness of the localization.

7.3 Construction of fractonic circuits

In order to construct our fractonic circuits, we need to define charges. The naive solution would be to use a spin-$\frac{1}{2}$ system, with spin-up being positive charge and spin-down being negative. However, in this case there is no obvious background. Instead, we can use a chain of spin-1 sites. The $Z_i = 1$ state will be a positive charge, the $Z_i = -1$ state a negative charge, and the $Z_i = 0$ state neutral. We will write these states as $+$, $-$, and 0, respectively.

Now we need to impose the conservation laws. Charge conservation is equivalent to conservation of Z_{tot}, so that's easy. In order to impose dipole conservation, we just need to make sure that each of our gates individually conserves dipole. However, that poses a problem because there are no non-trivial 2-site gates that conserve dipole. The solution is to consider 3-site unitary gates (or larger).

This gate set is still very restricted. Consider the initial state $+ - 0$. The only possible gates that conserve both Q and P are the identity and the gate $+ - 0 \leftrightarrow 0 + -$. The gate is defined by its action on states, with the assumption that it acts as the identity on all other states. A list of allowed gates is shown in Tab. 1. Note that there are very few 3-site gates. This raises concerns that the small number of gates affects the behavior of the circuit. We can allow more gates by having the gates each act on more sites, as in Tab. 1. Ref. [1] repeats their calculations for various size gates and finds the same results, so the number of allowed gates is not an issue.

Now that we have 3-site gates, there is one last complication to sort out, which is the placement of the gates. We cannot use the simple alternating structure of Fig.**??**. Instead, Ref. [1] uses an asymmetric structure, shown in Fig. 9. This architecture results in asymmetric lightcone velocities, but we will only look at spreading in one direction, so that will not be an issue.

Net charge	3-qudit gates	4-qudit gates
+2		$+\,0\,0\,+ \leftrightarrow 0\,+\,+\,0$ $0\,+\,0\,+ \leftrightarrow +\,-\,+\,+$ $+\,0\,+\,0 \leftrightarrow +\,+\,-\,+$
+1	$+\,-\,+ \leftrightarrow 0\,+\,0$	$0\,+\,0\,0 \leftrightarrow +\,-\,+\,0 \leftrightarrow +\,0\,-\,+$ $0\,0\,+\,0 \leftrightarrow +\,-\,0\,+ \leftrightarrow 0\,+\,-\,+$ $+\,0\,0\,0 \leftrightarrow 0\,+\,+\,-$ $0\,0\,0\,+ \leftrightarrow -\,+\,+\,0$ $-\,+\,0\,+ \leftrightarrow 0\,-\,+\,+$ $+\,+\,-\,0 \leftrightarrow +\,0\,+\,-$
0	$-\,+\,0 \leftrightarrow 0\,-\,+$	$0\,0\,0\,0 \leftrightarrow +\,-\,-\,+ \leftrightarrow -\,+\,+\,-$ $-\,+\,0\,0 \leftrightarrow 0\,-\,+\,0 \leftrightarrow 0\,0\,-\,+$ $+\,-\,0\,0 \leftrightarrow 0\,+\,-\,0 \leftrightarrow 0\,0\,+\,-$ $+\,0\,-\,0 \leftrightarrow 0\,+\,0\,-$ $0\,+\,0\,- \leftrightarrow +\,-\,+\,-$

Table 1: Allowed transitions in 3- and 4-site gates, sorted by total charge of the underlying states. Their are additional charge-0 transitions that can be found by swapping $+ \leftrightarrow -$ for the 2-state transitions. Furthermore each positive charge transitions have corresponding negative charge transitions found by swapping $+ \leftrightarrow -$. Figure from [1].

7.4 Numerical simulation

As in the rest of this essay, we will discuss numerical results that are taken from another paper, unsurprisingly [1]. We will individually show that the predictions listed in Sec. 7.2 are met.

The zeroth prediction was that of fracton localization. That can be shown by starting with an initially local fracton operator and calculating its evolution. The chosen operator is $IZIII\ldots$, where the only non-identity operator is on site 2. Recall that these are spin-1 systems, so

$$Z = \begin{pmatrix} 1 & 0 & 0 \\ 0 & 0 & 0 \\ 0 & 0 & -1 \end{pmatrix}. \tag{53}$$

The right-weight for this operator is shown in Fig. 10. Note that although the peak falls to around .5, it does not fall below that value, even at late time. Is this value significant?

This is in contrast to the evolution of an initially local dipole operator. Such an operator should be the sum of adjacent fracton operators, so that its eigenstates have positive charge at one state and negative charge at the next. The chosen operator in this case is

$$\frac{1}{2}\left(IZIII\ldots - IIZII\ldots\right) \tag{54}$$

Shouldn't it be $\frac{1}{\sqrt{2}}$? The initial $\frac{1}{2}$ ensures that $\sum_i \rho_R(i) = 1$. The time evolution of this operator is also shown in Fig. 10. Note that at late time $\sum_i \rho_R(i,t)$ is essentially flat. This shows that the dipole operator is not localized, and suggests further that the late-time behavior of the fracton operator is true localization.

To verify the first prediction, we need to move away from our familiar territory of operator spreading. The prediction is that charge density should be proportional to $\exp(R^2/2\sqrt{\pi}DCT)$. Recall that positive charge is represented by the +1 eigenstate of Z. Therefore the state with an initially local fracton is one where $\langle Z_i \rangle = 0$ for all i, except for one site j where $\langle Z_j \rangle = 1$. We will

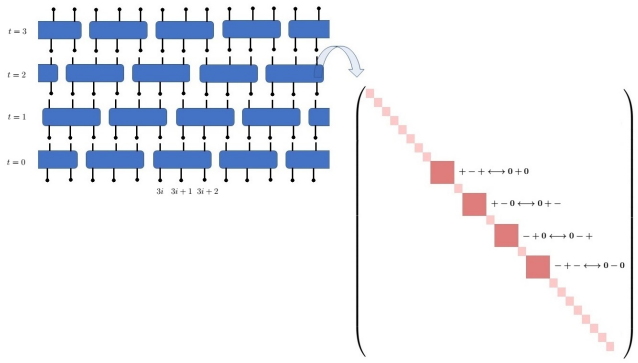

Figure 9: Architecture of the 3-site gate circuit. Each gate is a matrix of the form on the right, where each square is independently chosen from the applicable Haar distribution. The matrix is very sparse, corresponding to the small number of possible transitions. There are 4, as in Tab. 1 after adding the negative charge states. Figure from [1].

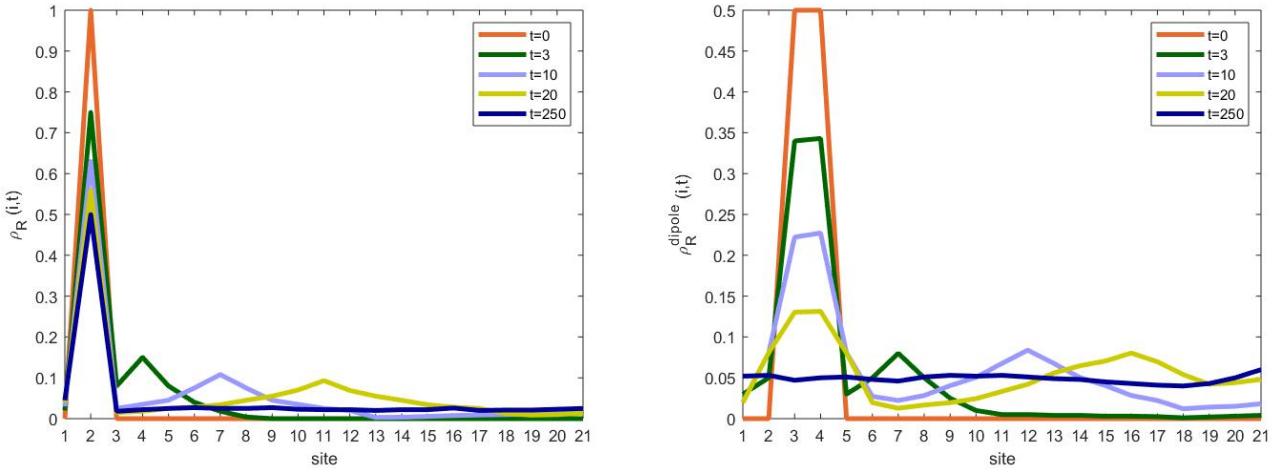

Figure 10: Operator spreading of the fracton operator and dipole operator, in a 21-site system with open boundary conditions. For the fracton, note the persistent peak at site 2, along with the propagating front. The dipole charge also has a propagating front, but the peak is nonexistent at late time. Figures from [1]

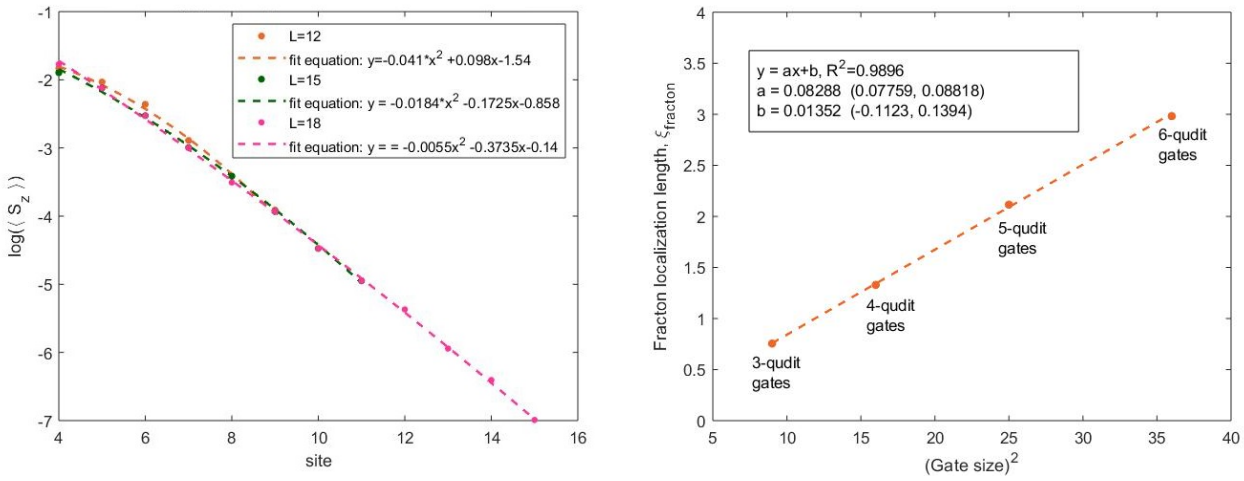

Figure 11: Left: Charge density at late times. If $\langle Z_i \rangle \sim \exp(-x^2)$, then this curve should be quadratic. It cannot be distinguished from a linear function, but the quadratic dependence is not ruled out. Right: Dependence of ξ_{fracton} on gate size. This plot more strongly confirms the second prediction of Sec. 7.2.

once again choose $j = 2$. Then we just have to show that $\langle Z_i \rangle \sim \exp(R^2/2\sqrt{\pi}DCT)$, $|i - j| = R$, where $\langle Z_i \rangle$ is evaluated with respect to a time-evolved state.

In Fig. 11 we show a plot of charge density at large t. The exponential dependence means that we can not distinguish between $\exp(-x^2)$ and $\exp(-x)$, so we count the first prediction as a maybe.

The second prediction also depends on the spreading of charge in a single fracton state. Here, however, we have to be able to change the diffusion constant D and random force T. We don't have many parameters left to vary in our system (the circuit is minimally structured) except for gate size. Ref. [1] shows that both D and T scale as (gate size)^2, so the second prediction reduces to

$$\xi_{\text{fracton}} \sim \sqrt{DT} \sim (\text{gate size})^2. \tag{55}$$

ξ_{fracton} can be extracted from the late-time charge density, as the half width at half maximum of the charge density peak. Fig. 11 also shows this relationship, confirming this prediction.

To test the last prediction, we head back to the operator spreading picture and focus on the fronts of the spreading operators.

8 Results and Conclusions

References

[1] S. Pai, M. Pretko, and R. M. Nandkishore, "Localization in fractonic random circuits," (2018), arXiv:1807.09776 .

[2] R. Nandkishore and D. A. Huse, "Many-body localization and thermalization in quantum statistical mechanics," Annual Review of Condensed Matter Physics **6**, 15–38 (2015).

[3] C. Gogolin and J. Eisert, "Equilibration, thermalisation, and the emergence of statistical mechanics in closed quantum systems," Reports on Progress in Physics **79**, 056001 (2016).

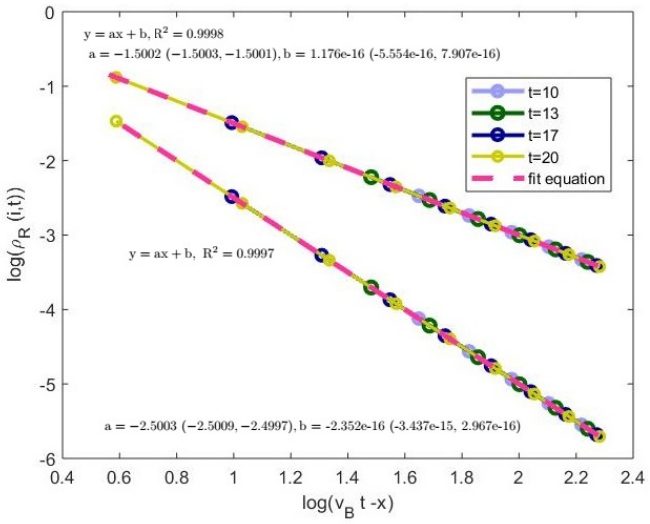

Figure 12: Behavior of the operator right weight behind the front. Each color plots For the dipole operator, ρ_R decreases with exponent $-3/2$ as in Sec. 5. For the fracton operator the exponent is $-5/2$ instead.

[4] A. Polkovnikov, K. Sengupta, A. Silva, and M. Vengalattore, "Colloquium: Nonequilibrium dynamics of closed interacting quantum systems," Reviews of Modern Physics **83**, 863–883 (2011).

[5] M. A. Cazalilla and M. Rigol, "Focus on dynamics and thermalization in isolated quantum many-body systems," New Journal of Physics **12**, 055006 (2010).

[6] T. Rakovszky, F. Pollmann, and C. W. von Keyserlingk, "Sub-ballistic growth of rnyi entropies due to diffusion," (2019), arXiv:1901.10502 .

[7] Y. Huang, "Dynamics of renyi entanglement entropy in local quantum circuits with charge conservation," (2019), arXiv:1902.00977 .

[8] C. Jonay, D. Huse, and A. Nahum, Coarse-grained dynamics of operator and state entanglement 1803.00089 .

[9] A. Pal and D. A. Huse, "Many-body localization phase transition," Phys. Rev. B **82**, 174411 (2010).

[10] V. Khemani, S. P. Lim, D. N. Sheng, and D. A. Huse, "Critical properties of the many-body localization transition," Phys. Rev. X **7**, 021013 (2017).

[11] C. von Keyserlingk, T. Rakovszky, F. Pollmann, and S. Sondhi, "Operator hydrodynamics, OTOCs, and entanglement growth in systems without conservation laws," Physical Review X **8** (2018), 10.1103/physrevx.8.021013.

[12] L. Zhang, V. Khemani, and D. A. Huse, "A floquet model for the many-body localization transition," Phys. Rev. B **94**, 224202 (2016).

[13] X. Chen, T. Zhou, D. A. Huse, and E. Fradkin, "Out-of-time-order correlations in many-body localized and thermal phases," Annalen der Physik **529**, 1600332 (2016).

[14] D. N. Page, "Average entropy of a subsystem," Phys. Rev. Lett. **71**, 1291–1294 (1993).

[15] L. Zhang, H. Kim, and D. A. Huse, "Thermalization of entanglement," Phys. Rev. E **91**, 062128 (2015).

[16] W. Brown and O. Fawzi, "Scrambling speed of random quantum circuits," ArXiv e-prints (2012), arXiv:1210.6644 [quant-ph] .

[17] A. Nahum, S. Vijay, and J. Haah, "Operator spreading in random unitary circuits," Physical Review X **8** (2018), 10.1103/physrevx.8.021014.

[18] V. Khemani, A. Vishwanath, and D. A. Huse, "Operator spreading and the emergence of dissipation in unitary dynamics with conservation laws," ArXiv e-prints (2017), arXiv:1710.09835 [cond-mat.stat-mech] .

[19] M. Pretko, "The fracton gauge principle," Physical Review B **98** (2018), 10.1103/physrevb.98.115134.

[20] M. Pretko and L. Radzihovsky, "Fracton-elasticity duality," Physical Review Letters **120** (2018), 10.1103/physrevlett.120.195301.

[21] D. Marenduzzo, "Advanced statistical physics," (2010).